THE JOURNAL OF PHYSICAL CHEMISTRY C

Article

pubs.acs.org/JPCC

Raman Scattering for Probing Semiconductor Nanocrystal Arrays with a Low Areal Density

Alexander G. Milekhin,*[,†,‡] Nikolay A. Yeryukov,[†] Larisa L. Sveshnikova,[†] Tatyana A. Duda,[†] Sergey S. Kosolobov,[†] Alexander V. Latyshev,[†,‡] Nikolay V. Surovtsev,[§] Sergey V. Adichtchev,[§] Cameliu Himcinschi,[⊥] Eduard I. Zenkevich,[¶] Wen-Bin Jian,[&] and Dietrich R. T. Zahn[#]

[†]A.V. Rzhanov Institute of Semiconductor Physics, Pr. Lavrentieva, 13, Novosibirsk 630090, Russia

[‡]Novosibirsk State University, Pirogov Strasse 2, 630090, Novosibirsk, Russia

[§]Institute of Automation and Electrometry, Koptyug Avenue 1, 630090, Novosibirsk, Russia

[⊥]Institut für Theoretische Physik, TU Bergakademie Freiberg, Leipziger Strasse 23, 09596, Freiberg, Germany

[¶]National Technical University of Belarus, Nezavisimosti Avenue 65, 220013 mink, Belarus

[&]Department of Electrophysics, NCTU, Hsinchu 30010, Taiwan

[#]Semiconductor Physics, Chemnitz University of Technology, D-09107 Chemnitz, Germany

Supporting Information

ABSTRACT: We present a study of resonant and surface enhanced Raman scattering by arrays of nanocrystals (cadmium sulfide CdS, lead selenide PbSe, and zinc oxide ZnO) with various areal density fabricated by using the Langmuir−Blodgett technique and colloidal chemistry. Resonant Raman scattering by transverse, longitudinal, and surface optical (TO, LO, and SO) phonons and their overtones up to ninth order was achieved for nanocrystal (NC) arrays by adjusting the laser energy to that of the interband transitions. The resonance enhancement allowed a Raman response from arrays of NCs with a low areal density (down to 10 PbSe NCs per 1 μm^2) to be measured. An enhancement of Raman scattering by LO and SO modes in CdS NC arrays with a low areal density by a factor of about 730 was achieved due to the resonant surface enhanced Raman scattering effect.

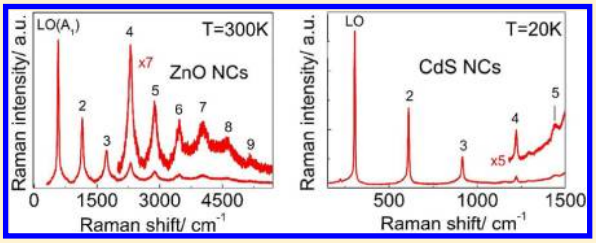

INTRODUCTION

Most of the published data on phonons in nanocrystals or quantum dots are related to Raman scattering in dense NC arrays.[1−3] Significant efforts were made to understand interference of acoustical phonons,[1,3] confinement of acoustical and optical phonons,[1−9] and quantization of the spectrum of surface and interface optical phonons[10−12] in NC superlattices and single layer NC arrays. It was also shown theoretically that a single NC should reveal a rich phonon spectrum.[13,14] Despite remarkable interest in the vibrational spectra of NC arrays the experimental study of phonons in NC arrays especially of a low areal density down to a single NC remains a challenge. The Raman response of a NC array is an average of that of single NCs with different sizes. Consequently the effects of phonon confinement in a single NC are smeared out. Therefore the vibrational spectrum of single NCs still remains unknown. The relatively small Raman cross-section of such NC arrays complicates the observation of phonon modes in NCs. Recently, Sarkar et al. and Chilla et al.[15,16] reported the observation of features in photoluminescence experiments which were attributed to optical and acoustic phonons in a single NCs. However, the challenge of experimentally determining the phonon spectrum of a single NC by using Raman scattering experiments has not yet been solved in general.

The aim of this study is the elaboration of appropriate approaches for increasing the Raman efficiency of NCs. One of the possibilities is to employ resonant Raman scattering (RRS) when the energy of the incident laser light matches that of interband electronic transitions in the NCs. This approach is widely used for a variety of NC systems.[17−19] An alternative approach is the realization of surface enhanced Raman scattering (SERS) when the energy of the incident laser light is close to the surface plasmon energy in noble metal nanoclusters which are intentionally introduced in NC arrays.[20−22] Resonant SERS (SERRS), which takes place by coincidence of the energies of laser light, surface plasmons in metal nanoclusters, and interband transitions in NCs, combines the advantages of both methods. Here, we consider all three issues.

Received: November 14, 2011
Revised: July 18, 2012
Published: July 23, 2012

dx.doi.org/10.1021/jp210720v | J. Phys. Chem. C 2012, 116, 17164−17168

EXPERIMENTAL SECTION

It was already shown that high-quality semiconductor NC (CdS, CuS, ZnS, PbS, and ZnO) arrays can be formed by using the Langmuir−Blodgett (LB) technique.[5] The process of NC formation can be briefly described as follows. At the first stage high-quality LB films of metal (Ag, Cd, Cu, Zn, and Pb) behenates are deposited on quartz or Si substrates covered by a 100 nm thick Au or Pt layer. The typical thickness of LB films that are used to form dense NC arrays is about 400 monolayers (ML). LB films with nominal thicknesses below 10 ML are used for the formation of NC arrays of a low areal density and for further comparison with dense NC arrays. The reaction of the behenates with gaseous H_2S results in the formation of NCs of metal sulfides. Free-standing NCs were obtained after removing the organic matrix by thermal annealing under vacuum or in an inert atmosphere at temperatures between 100 and 200 °C. Atomic force microscopy experiments show that an LB film of thickness 440 ML after thermal annealing leads to formation of dense CdS NC arrays with the nominal thickness of about 70 nm. Samples with CdS NCs were denoted as Cd*X*, where *X* = 440, 60, 10, 8, 6, 4 is the thickness (in MLs) of the initial cadmium behenate film used for formation of CdS NCs. With increasing *X* the areal density of NCs increases while the NC diameter remains constant (of about 4−6 nm[1]).

Free-standing ZnO NCs were formed as a result of annealing of either Zn behenate films or ZnS NCs at 600 °C in air. In this paper we focus on the study of CdS and ZnO NC arrays of different areal densities. For SERS experiments Ag nanocluster films were deposited on the surface of NCs also by the LB technology[23] or vacuum evaporation. After deposition of Ag nanoclusters samples Cd*X* were labeled as Cd*X*Ag. The size of Ag clusters determined from scanning electron microscopy (SEM) images is in the range from 10 to 20 nm. The size uniformity for each sample amounts to about 50%. PbSe NCs were prepared using a high-temperature organic solution approach[24−26] on graphite substrates. Highly oriented pyrolytic graphite (HOPG) was chosen as a substrate due to good thermal and electric conductivities. From one side, graphite withdraws effectively the heat from NCs induced by the intense laser light. From the other side, graphite is well suited for SEM measurements because of its atomically flat surface and high electric conductivity. SEM experiments were carried out to determine the size and areal density of NCs using a scanning electron microscope FIB, 1540XB, Cross Beam, Carl Zeiss. SEM images were obtained at the beam voltage of 20 kV with the probe size of 1.1 nm.

The crystal structure of the NCs prepared using the LB technology was determined from X-ray diffraction measurements.[5] It was established that ZnO and CdS NCs have a hexagonal crystal structure. ZnO NCs have a lateral size of approximately 40 nm and a height of 4−6 nm. The average diameter of monodisperse PbSe NCs was determined to be 15 nm on the basis of SEM images, while the standard deviation was estimated to be 10%. The focused ion beam (FIB) technique with further control by SEM was used to form square mesa structures with a size of 4 × 4 μm^2. As a result mesa structures with different areal density of NCs were prepared which were further investigated in micro-Raman experiments.

UV−vis absorption spectra of NCs grown on quartz substrates were recorded with use of a UV spectrometer Shimadzu UV-31000 in the wavelength range of 200−800 nm at room temperature.

Raman experiments were carried out with Jobin Yvon Dilor XY800, LabRam-UV, and T64000 spectrometers in back-scattering geometry analyzing nonpolarized scattered light. Ar^+, Kr^+, and HeCd lasers were used as excitation sources in the wavelength range from 752.5 to 325 nm. In the macro-geometry the incident laser light with a power of 100 mW or less was focused by a spherical lens to reach the laser spot diameter of about 50 μm or by a cylindrical lens to get a focused laser stripe with a size of about 50 × 1000 μm^2 to minimize sample heating. Using a micro-Raman setup the incident laser light was focused with a spot size diameter of 1 μm on the surface of a NC sample or a mesa structure.

RESULTS AND DISCUSSION

Resonant Raman Scattering of Dense NC Arrays. Raman spectra of arrays of closely packed PbS, CuS, Ag_2S, ZnS, and ZnO NCs were investigated in our previous study[5] with a wide range of wavelengths of the laser light to satisfy both resonant and nonresonant conditions. The most intensive Raman scattering by optical phonons in dense PbS, CuS, Ag_2S, and ZnS NC arrays is observed when the energy of interband transitions of NCs is close to resonance with the laser excitation energy. Out of resonance the Raman signal drops down by up to 2 orders of magnitude. The resonant and nonresonant Raman spectra for ZnO NCs differ significantly not only in the sense of the mode intensity but also in the mode symmetry.[28] Figure 1 shows the comparison of the Raman spectra in dense

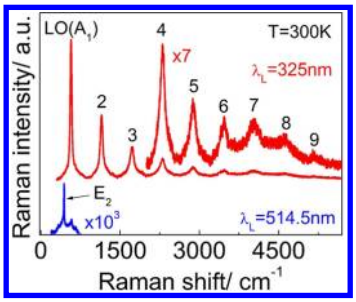

Figure 1. Raman spectra of dense ZnO NC array measured with excitation wavelengths of (upper curve) 325 nm (resonant conditions) and (bottom curve) 514.5 nm (non-resonant conditions). The numbers indicate the corresponding overtones of the $LO(A_1)$ phonon modes in the resonant Raman spectrum (upper curve).

ZnO NC array measured at 514.5 and 325 nm which are far from and close to the resonance with interband transitions in NCs, respectively. The most pronounced phonon mode seen in the nonresonant Raman spectra of ZnO NCs is the E_2 phonon mode at 437 cm^{-1} (dashed line) while a mode at 574 cm^{-1} and its overtones (up to ninth order) are active in resonant conditions (solid lines). The mode at 574 cm^{-1} refers to $LO(A_1)$ phonons in the ZnO NCs.[28] Nine overtones observed indicates the excellent crystalline and optical quality of the NCs. Similar spectra but measured at low temperature (77 K) demonstrating multiple phonon Raman scattering up to eighth order were also observed in nanocrystalline ZnO.[29] The intensity of Raman scattering by ZnO NC arrays is enhanced by a factor of about 10^3 in resonant conditions. This allows Raman investigations of ZnO NC arrays of low area densities to be performed. The Raman study of NC arrays of low areal densities requires an intensive power of laser irradiation of the sample which can cause degradation of ZnO NCs. Therefore, PbSe NCs deposited on graphite substrate were chosen for the

dx.doi.org/10.1021/jp210720v | J. Phys. Chem. C 2012, 116, 17164−17168

study of NC arrays of low areal density. From one side, these NCs were found to be more resistant against an intensive laser irradiation. From the other side, the morphology of the NC arrays with various areal densities can be easily determined by SEM due to a heavy mass of lead atoms.

Resonant Micro-Raman Scattering of NC Arrays with Low Areal Density. Figure 2 shows the SEM images of mesa

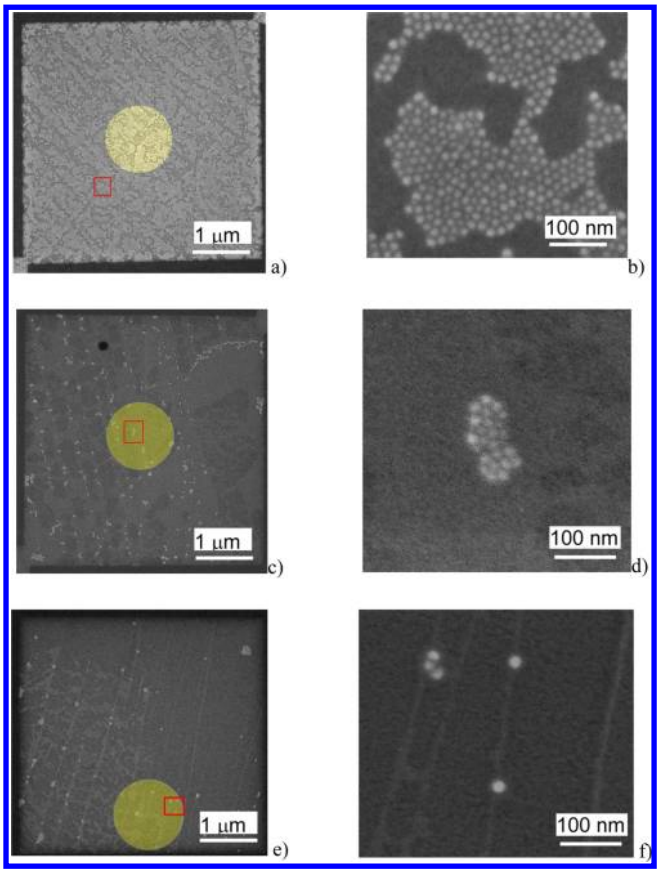

Figure 2. SEM images of mesa structures having different areal densities of PbSe NCs (light spots): (a, b) 1.7×10^3 NCs/μm^2; (c, d) 100 NCs/μm^2; and (e, f) 15 NCs/μm^2. The rectangular areas shown in panels a, c, and e are plotted enlarged in panels b, d, and f, respectively. The laser spots (illuminated areas) are shown schematically by circles.

structures with PbSe NC arrays of various areal densities. One can see from panels a and b of Figure 2 that PbSe NCs are densely packed in a single NC layer, while the SEM images shown in panels c and d of Figure 2 reveal ten times lower areal density of NCs. Finally, the SEM images of the mesa structure shown in panels e and f of Figure 2 demonstrate extremely low density of NCs so that only a few PbSe NCs (about ten) can be simultaneously illuminated in the micro-Raman experiment. The area illuminated by the laser light is demonstrated in Figure 2 by light circles of 1 μm diameter. In addition, the as-prepared structure with a thick 3-dimensional layer of PbSe NCs was used for comparison (SEM images of the structure are not shown in the figures).

Micro-Raman spectra of as-prepared PbSe NC structures and the mesa structures with different NC areal density measured with a Dilor XY-800 spectrometer and the laser line at 647.1 nm (1.92 eV) and a Labram spectrometer with 532.2 nm (2.33 eV) are presented in Figure 3 (curves 1–4). The excitation

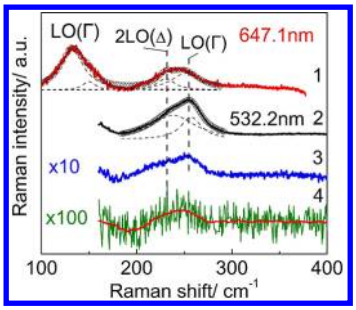

Figure 3. Room temperature micro-Raman spectra of (curve 1) 3-dimensional PbSe NC layers measured with 647.1 nm and (curves 2–4) PbSe NC single layers with different NC densities measured with 532.2 nm. Open circles and thin dashed lines represent the results of fitting with Lorentzian line shapes. Vertical dashed lines are guides to the eye.

energies are close to the energies of electronic transitions in PbSe observed at 1.95 and 2.19–2.51 eV.[30] The Raman spectra measured with the Dilor XY-800 spectrometer can be recorded down to the acoustical spectral range (100 cm^{-1}). However, the use of the triple monochromator reduces the intensity of the phonon response from PbSe NCs. The employment of a Labram spectrometer with a single monochromator enhances the phonon response but reduces the accessible spectral range at the low frequency side due to the edge filter used for the elimination of the elastically scattered laser light (Figure 3, curves 2–4). It is important to notice that the Raman spectra shown in Figure 3 (curves 2–4) were recorded from the areas shown in Figure 2 (images a, c, and e, respectively).

The spectrum of PbSe NCs measured with a triple spectrometer in the macro-Raman geometry reveals two broad asymmetrical features near 135 and 250 cm^{-1} (Figure 3, curve 1). We suppose that each feature consists of two phonon modes. The phonon frequencies of these modes are determined from the best fit with Lorentzian line shapes. The results from the curve fitting of the Raman spectra are shown in Figure 3. The peaks at 132 and 149 cm^{-1} are attributed to first-order Raman scattering by LO phonons in PbSe NCs from the Γ-point of the Brillouin zone[31,32] and to contributions of higher-order Raman scattering,[32] respectively. The feature in Figure 3 (curves 1 and 2) located near 250 cm^{-1} is fitted by two Lorentzian curves centered at 230 and 251 cm^{-1} and 238 and 257 cm^{-1}, assigned to second order Raman scattering (2LO) from different points of the Brillouin zone (Δ and Γ). This assignment is based on literature data for PbSe of the doublet structure with maxima at 243 and 288 cm^{-1},[33] and 244 and 265 cm^{-1}.[34] One can see from Figure 3 (curve 4) that the Raman phonon response is observed even for the structure with only a few PbSe NCs. Note that the Raman spectrum (curve 1) was scaled and its intensity cannot be directly compared with that of the Raman spectra of NCs (curves 2–4). However, the decreasing relative intensity of the Raman signal (130/90/7 taken from Figure 3, curves 2–4) follows the decrease of the NC areal density (1700/100/15 NCs/μm^2 taken from Figure 2, images a, c, and e, respectively). The deviations can be caused by inhomogeneous laser illumination of NCs over the investigated area.

Surface-Enhanced Raman Scattering of CdS NC Arrays. Enhancement of Raman scattering by optical phonons was achieved by the deposition of Ag nanoclusters (NCs) on the surface of dense CdS NC arrays.[20] Figure 4 shows the Raman spectra of the structures containing free CdS NCs with

dx.doi.org/10.1021/jp210720v | J. Phys. Chem. C 2012, 116, 17164–17168

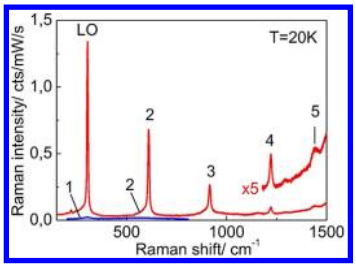

Figure 4. Raman spectra of samples containing free CdS NCs (samples Cd440 and Cd440Ag) without and with Ag NCs (curves 1 and 2, respectively) excited with the 476.5 nm laser line. The numbers mark the corresponding overtones of the LO phonon from CdS NCs seen in the SERS spectrum.

and without Ag NCs (samples Cd440Ag and Cd440, respectively). The Raman spectrum of the sample Cd440 (curve 1 in Figure 4) reveals only a weak feature near 300 cm^{-1} associated with the LO phonons localized in CdS NCs. Deposition of Ag NCs on the surface of NC layers leads to a strong enhancement (150-fold) of the Raman intensities. The enhancement factor can be easily calculated as

$$E_{Cd440Ag} = \frac{I_{Cd440Ag}}{I_{Cd440}} \quad (1)$$

where $I_{Cd440Ag}$ and I_{Cd440} are the intensity of LO phonon scattering where the subscripts denote the sample numbers. The Raman spectrum of sample Cd440Ag (curve 2 in Figure 4) exhibits several intensive peaks related to first-order Raman scattering by LO phonons from CdS NCs at 304 cm^{-1} and their overtones up to fifth order with spacings approximately equal to the LO phonon energy in CdS NCs. The shape asymmetry of the LO phonon line is due to SO phonons in the NCs occurring at about 280 cm^{-1}.[35] The measurement of the SERS intensity of the LO phonon line as a function of the thickness of the CdS NC layers reveals that only the first topmost NC layers in the vicinity of Ag NCs contribute to the SERS effect while underlying CdS NCs are responsible for the ordinary Raman signal.[20] Determination of SERS enhancement factor by eq 1 for samples Cd*X*Ag with $X < 100$ needs to be corrected because the Raman signal from samples Cd*X* with $X < 100$ is below the detection limit of the experiment. Therefore, for samples Cd*X*Ag (with $X < 100$) the SERS enhancement factor was modified as following

$$E_{CdXAg} = E_{Cd440Ag}\frac{I_{CdXAg}/d_{CdXAg}}{I_{Cd440Ag}/d_{Cd440Ag}} \quad (2)$$

where $E_{Cd440Ag} = I_{Cd440Ag}/I_{Cd440}$ and $d_{CdXAg}/d_{Cd440Ag}$ is the thickness ratio of CdS NC layers in samples Cd*X*Ag and Cd440Ag, respectively.

To determine the enhancement factor as a function of the wavelength, SERS spectra of CdS NCs were measured with different laser excitation wavelengths. The energy dependence of the enhancement factor shows clear resonance behavior with a maximum the energy position of which depends on the surface plasmon resonance (SPR) energy. The SPR energy controlled by optical absorption of Ag NCs (curves 1−3 in Figure 5a) was tuned to the energy of interband electronic transitions in NCs by the variation of the NC size. The width of the absorption features is most probably determined by size distribution of Ag nanoclusters but was not directly evident from SEM images because of their relatively small size (10−20

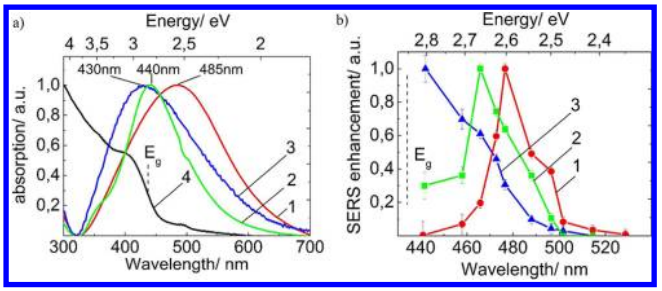

Figure 5. (a) Absorption spectra of Ag NCs having different energy of SPR (curves 1−3) and of CdS NCs (curve 4). (b) Normalized SERS enhancement by optical phonons measured for samples Cd440Ag, Cd60Ag, and Cd20Ag (curves 1, 2, and 3, respectively) having different SPR energies determined from absorption spectra shown in panel a (curves 1−3).

nm). The energy position of the interband transitions determined from absorption spectra of CdS NCs (curve 4 in Figure 5a) amounts to 2.85 eV (435 nm). One can see from Figure 5a that the energy of SPR coincides with the energy of interband electronic transitions in NCs and therefore the conditions for SERRS are achieved.

Figure 5b shows the SERS enhancement factors determined by eqs 1 and 2 for samples Cd440Ag, Cd60Ag, and Cd20Ag (curves 1−3, respectively) with Ag NCs having different SPR energies. The maximum of SERS enhancement (Figure 5b) tends to follow the maximal SPR absorption and reaches a value of 730 at 2.8 eV for sample Cd20Ag, which represents a single layer NC array.

SERRS spectra were measured for CdS NC arrays in the spectral range of LO phonons even with a lower areal density. Figure 6a shows the SERRS spectra of the CdS NC arrays with

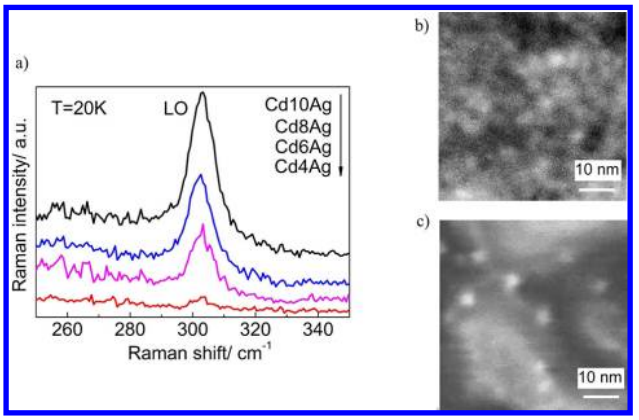

Figure 6. (a) SERRS spectra of CdS NC arrays with various areal densities (samples Cd10Ag, Cd8Ag, Cd6Ag, and Cd4Ag) excited with the 457.9 nm laser line. (b and c) SEM images (50 × 50 nm^2) of samples Cd10 and Cd4, respectively. The light spots are CdS NCs.

different areal densities of NCs (samples Cd10Ag, Cd8Ag, Cd6Ag, and Cd4Ag). Panels b and c of Figure 6 show typical SEM images (50 × 50 nm^2) of samples Cd10 and Cd4. In sample Cd10, CdS NCs form a dense NC monolayer while only a few NCs can be seen from the SEM image of sample Cd4 (Figure 6c). The intensity of Raman scattering by LO phonons localized in CdS NCs decreases with decreasing of NCs and remains visible even for sample Cd4Ag. The areal density of CdS NCs can be estimated from the SEM images. For sample Cd10 it amounts to about 4 × 10^{12} cm^{-2} while the

dx.doi.org/10.1021/jp210720v | J. Phys. Chem. C 2012, 116, 17164−17168

areal density of NCs in sample Cd4 is 1 order of magnitude lower (4×10^{11} cm^{-2}). Samples Cd6 and Cd8 have intermediate densities (SEM images are not shown here) of NCs (about 3×10^{11} and 1×10^{12} cm^{-2}, respectively). One can see from Figure 6 that the Raman signal is proportional to the areal density of NCs. About 10 NCs contribute to the Raman signal from the area shown in Figure 6c and, thus, CdS NC arrays with areal density down to 4×10^{11} cm^{-2} can be probed by SERS. In these experiments the Raman scattering signal is recorded from an area with a diameter of about 50 μm where the laser spot is focused by a spherical lens. It is worth mentioning that the degradation of CdS NCs under laser illumination prevents the observation of the phonon response of CdS NC arrays with low areal density in a micro-Raman configuration at temperatures from 300 to 77K.

CONCLUSION

We discussed various approaches which can be used for studying Raman scattering in NC arrays of low areal density. The significant enhancement of Raman scattering by optical phonon modes localized in NCs is observed for a number of NC materials under resonant conditions. The ability of Raman spectroscopy to probe the phonon spectrum of NC arrays with ultralow areal density well controlled by SEM is demonstrated and the phonons of about a dozen PbSe NCs are probed. Conditions for SERS and SERRS by optical phonons from CdS NCs are realized and the enhancement factor of about 730 is achieved.

ASSOCIATED CONTENT

Supporting Information

SEM characterization of Ag clusters having different size and information on the energy of surface plasmon absorption in Ag clusters. This material is available free of charge via the Internet at http://pubs.acs.org.

AUTHOR INFORMATION

Corresponding Author

*E-mail: milekhin@thermo.isp.nsc.ru. Tel: +7-383-316-60-54. Fax: +7-383-333-27-71.

Notes

The authors declare no competing financial interest.

ACKNOWLEDGMENTS

This work was supported in part by the RFBR (grant nos. 11-02-90427-Ukr_f_a and 11-02-91348-NNIO_a), the Presidium of RAS-2010 (grant no. 24.27), SB RAS (grant no. 134), DFG (grant no. Za146/22-1), and IRTG (Grant GRK 1215). Raman experiments were partially carried out at the Research and Educational Center at the Novosibirsk State University.

REFERENCES

(1) Milekhin, A.; Tenne, D. A.; Zahn, D. R .T. *Nanocrystals and Nanowires*; Bandyopadhyay, S., Nalwa, H. S., Eds.; American Scientific Publishers: Stevenson Ranch, CA, 2003; Chapter 10, pp 375−419.

(2) Wagner, V.; Geurts, J.; Kiefer, W. *Nanocrystals and Nanowires*; Bandyopadhyay, S., Nalwa, H. S., Eds.; American Scientific Publishers: Stevenson Ranch, CA, 2003; Chapter 7, pp 241−302.

(3) Mlayah, A.; Groenen, J. *Light Scattering in Solid IX*; Cardona, M., Merlin, R., Eds.; 2007, ; Springer-Verlag Berlin: Heidelberg, Germany, 2007; *Topics in Applied Physics*, Vol. *108*, 237−314.

(4) Tenne, D. A.; Haisler, V. A.; Toropov, A. I.; Bakarov, A. K.; Gutakovsky, A. K.; Zahn, D. R. T.; Shebanin, A. P. *Phys. Rev. B* **2000**, *61*, 13785−13790.

(5) Milekhin, A. G.; Sveshnikova, L. L.; Duda, T. A.; Surovtsev, N. V.; Adichtchev, S. V.; Azhniuk, Yu. M.; Himcinschi, C.; Kehr, M.; Zahn, D. R. T. *J. Phys.: Conf. Ser.* **2010**, *245*, 012045−1−4.

(6) Milekhin, A. G.; Toropov, A. I.; Bakarov, A. K.; Schulze, S.; Zahn, D. R. T. *JETP Lett.* **2006**, *83*, 505−508.

(7) Milekhin, A. G.; Nikiforov, A. I.; Pchelyakov, O. P.; Rodrigues, A. G.; Galzerani, J. C.; Zahn, D. R. T. *JETP Lett.* **2005**, *81*, 30−33.

(8) Milekhin, A. G.; Nikiforov, A. I.; Pchelyakov, O. P.; Schulze, S.; Zahn, D. R. T. *Nanotechnology* **2002**, *13*, 55−58.

(9) Azhniuk, Yu. M.; Milekhin, A. G.; Gomonnai, A. V.; Lopushansky, V. V.; Yukhymchuk, V. O.; Schulze, S.; Zenkevich, E. I.; Zahn, D. R. T. *J. Phys.: Condens. Matter* **2004**, *16*, 9069−9082.

(10) Milekhin, A. G.; Toropov, A. I.; Bakarov, A. K.; Tenne, D. A.; Zanelatto, G.; Galzerani, J. C.; Schulze, S.; Zahn, D. R. T. *Phys. Rev. B* **2004**, *70*, 085313−1−5.

(11) Comas, F.; Trallero-Giner, C.; Studart, N.; Marques, G. E. *J. Phys.: Condens. Matter* **2002**, *14*, 6469−6481.

(12) Ladanov, M. Yu; Milekhin, A. G.; Toropov, A. I.; Bakarov, A. K.; Gutakovskii, A. K.; Tenne, D. A.; Schulze, S.; Zahn, D. R. .T *J. Exp. Theor. Phys.* **2005**, *101*, 554−561.

(13) Lua, D.; Zhu, B.-F. *Solid State Commun.* **2000**, *115*, 313−317.

(14) Roca, E.; Trallero-Giner, C.; Cardona, M. *Phys. Rev. B* **1994**, *49*, 13704−13711.

(15) Sarkar, D.; van der Meulen, H. P.; Calleja, J. M.; Pierz, K. *Phys. Rev. B* **2005**, *71*, 081302(R)-1−4.

(16) Chilla, G.; Kipp, T.; Menke, T.; Heitmann, D. *Phys. Rev. Lett. B* **2005**, *100*, 057403-1−4.

(17) Kumar, B.; Gong, H.; Chow, S. Y.; Tripathy, S.; Hua, Y. *Appl. Phys. Lett.* **2006**, *89*, 071922-1−3.

(18) Saviot, L.; Champagnon, B.; Duval, E.; Ekimov, A. I. *Phys. Rev. B* **1998**, *57*, 341−346.

(19) Dzhagan, V.; Valakh, M. Ya.; Kolny-Olesiak, J.; Lokteva, I.; Zahn, D. R. T. *Appl. Phys. Lett.* **2009**, *94*, 243101-1−3.

(20) Milekhin, A. G.; Sveshnikova, L. L.; Duda, T. A.; Surovtsev, N. V.; Adichtchev, S. V.; Zahn, D. R. T. *JETP Lett.* **2008**, *88*, 799−801.

(21) Hugall, J. T.; Baumberg, J. J.; Mahajan, S. *Appl. Phys. Lett.* **2009**, *95*, 141111-1−3.

(22) Shan, G.; Xu, L.; Wang, G.; Liu, Y. *J. Phys. Chem. C* **2007**, *111*, 3290−3293.

(23) Surovtsev, N. V.; Adichtchev, S. V.; Duda, T. A.; Pokrovsky, L. D.; Sveshnikova, L. L. *J. Phys. Chem. C* **2010**, *114*, 4803−4807.

(24) Murray, C. B.; Sun, S.; Gaschler, W.; Doyle, H.; Betley, T. A.; Kagan, C. R. *IBM J. Res. Dev.* **2001**, *45*, 47−56.

(25) Chen, F.; Stokes, K. L.; Zhou, W.; Fang, J.; Murray, C. B. *Mater. Res. Soc. Symp. Proc.* **2002**, *691*, G10.2.1−G10.2.16.

(26) Cho, K.-S.; Talapin, D. V.; Gaschler, W.; Murray, C. B. *J. Am. Chem. Soc.* **2005**, *127*, 7140−7147.

(27) Milekhin, A. G.; Eryukov, N. A.; Sveshnikova, L. L.; Duda, T. A.; Zen'kevich, E. I.; Kosolobov, S. S.; Latyshev, A. V.; Himcinshi, C.; Surovtsev, N. V.; Adishchev, S. V.; et al. *J. Exp. Theor. Phys.* **2011**, *113* (6), 983−991.

(28) Alim, K. A.; Fonoberov, V. A.; Balandin., A .A. *Appl. Phys. Lett.* **2005**, *86*, 053103−1−3.

(29) Kumar, B.; Gong, H.; Chow, S. Y.; Tripathy, S.; Hua, Y. *Appl. Phys. Lett.* **2006**, *89*, 071922−1−3.

(30) Albanesi, E. A.; Okoye, C. M. I.; Rodriguez, C. O.; Peltzer y Blanca, E. L.; Petukhov, A. G. *Phys. Rev. B* **2000**, *61*, 16589−16595.

(31) Yang, A.-L.; Wu, H.-Z.; Li, Z.-F.; Qiu, D.-J.; Chang, Y.; Li, J.-F.; McCann, P. J.; Fang, X. M. *Chin. Phys. Lett.* **2000**, *17*, 606−608.

(32) Ovsyannikov, S. V.; Ponosov, Y. S.; Shchennikov, V. V.; Mogilenskikh, V. E. *Phys. Status Solidi C* **2004**, *1*, 3110−3113.

(33) Chen, J.; Shen, W. Z. *J. Appl. Phys.* **2006**, *99*, 013513−1−5.

(34) Upadhyaya, K. S.; Yadav, M.; Upadhyaya, G. K. *Phys. Status Solidi B* **2002**, *229*, 1129−1138.

(35) Milekhin, A.; Friedrich, M.; Zahn, D. R. T.; Sveshnikova, L.; Repinsky, S. *Appl. Phys. A: Mater. Sci. Process.* **1999**, *69*, 97−100.